Position of Transmembrane Helix 6 Determines Receptor G Protein Coupling Specificity

Alexander S. Rose,[†,‡] Matthias Elgeti,[†] Ulrich Zachariae,[§] Helmut Grubmüller,[‖] Klaus Peter Hofmann,[†,⊥] Patrick Scheerer,[†,#] and Peter W. Hildebrand[†,‡]

[†]Institut für Medizinische Physik und Biophysik, [‡]AG ProteiInformatics, and [#]AG Protein X-ray Crystallography, Charité Universitatsmedizin Berlin, Charitéplatz 1, 10117 Berlin, Germany

[§]Division of Computational Biology, College of Life Sciences, and Division of Physics, School of Engineering, Physics and Mathematics, University of Dundee, Dow Street, Dundee DD1 5EH, U.K.

[‖]Department of Theoretical and Computational Biophysics, Max-Planck-Institute for Biophysical Chemistry, D-37077 Göttingen, Germany

[⊥]Centre of Biophysics and Bioinformatics, Humboldt-Universitat zu Berlin, Invalidenstrasse 42, D-10115 Berlin, Germany

Supplemental Information Figures

Table S1

System	Simulations	Length
RhR*	1x 400 ns, 4x 200 ns	1.2 µs
RhR*·GtαCT$_{19}$	5x 200 ns	1 µs
RhR*·GtαCT$_{11}$	1x 400 ns, 4x 200 ns	1.2 µs
RhR*·GsαCT$_{19}$	5x 200 ns	1 µs
β_2AR*	1x 400 ns, 4x 200 ns	1.2 µs
β_2AR*·Gs$\alpha\beta\gamma$	5x 200 ns	1 µs
β_2AR*·GsαCT$_{19}$	1x 400 ns, 4x 200 ns	1.2 µs
β_2AR*·GsαCT$_{11}$	10x 500 ns	5 µs
β_2AR*·GiαCT$_{19}$	3x 600 ns, 8x 200 ns, 10x 100 ns	4.4 µs
		17.2 µs

Overview of performed MD simulations. Each row lists the system, the length and count of simulations, and the overall per system simulation time. The total simulation time is 17.2 µs.

Figure S1

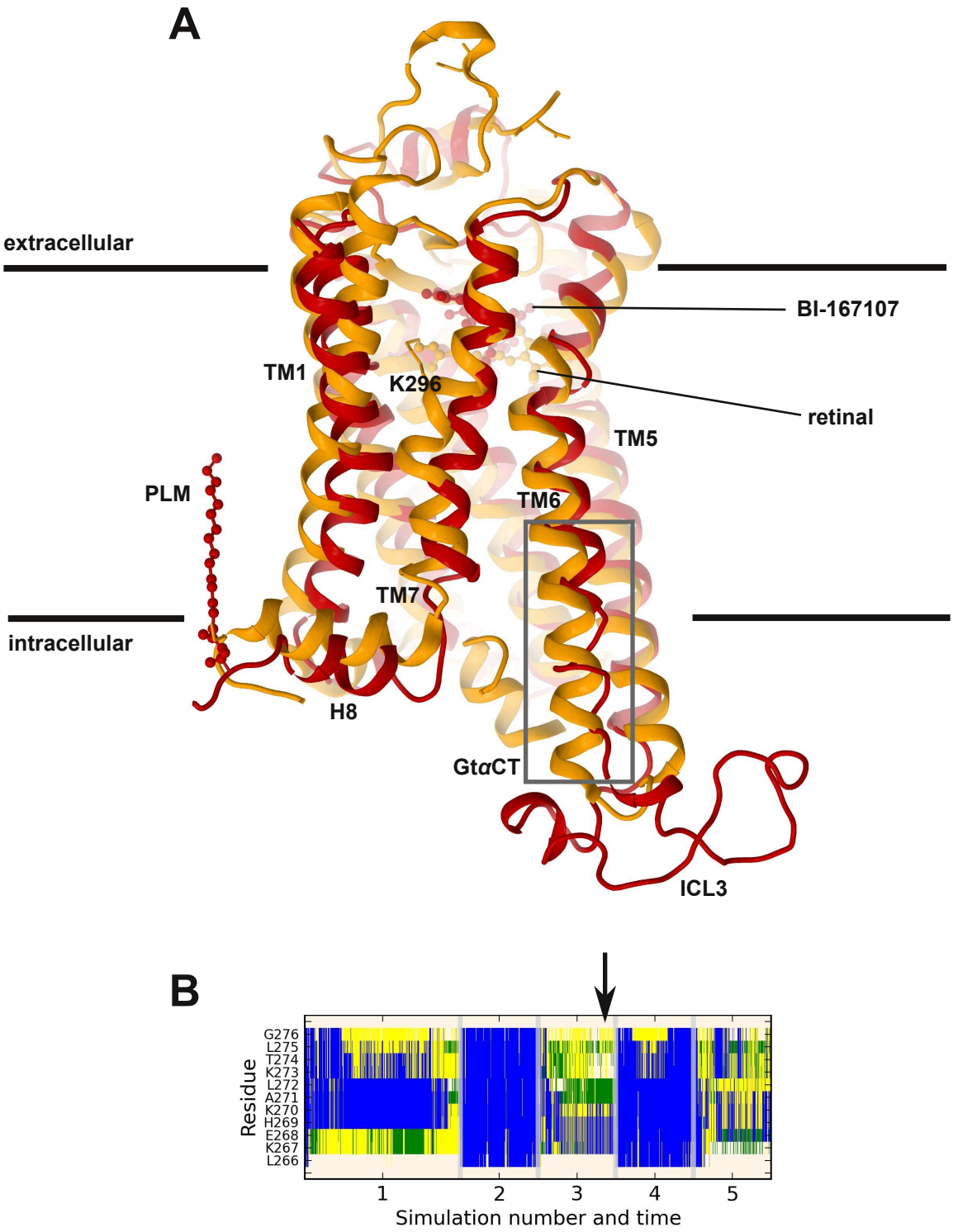

(**A**) Superposition of the RhR*·Gt*α*CT crystal structure (orange, PDB entry 3PQR) with a snapshot from the MD simulation of uncomplexed β_2AR* (red). Note the similarity of the TM6 tilt at the intracellular side. The grey box denotes the part of TM6 analyszed in B. (**B**) Time series showing the secondary structure assignment of the intracellular TM6 region of β_2AR* as calculated with DSSP (W. Kabsch, C. Sander, Biopolymers 1983, 22, 2577–2637.). The observed structure types are α-helix (blue), 3_{10}-helix (grey), turn (yellow), coil (white) or bend (green). The black arrow denotes from which simulation and at what time the β_2AR* structure shown in A was taken. The plot shows the data of multiple MD simulations, each between 200 and 400 ns long.

Figure S2

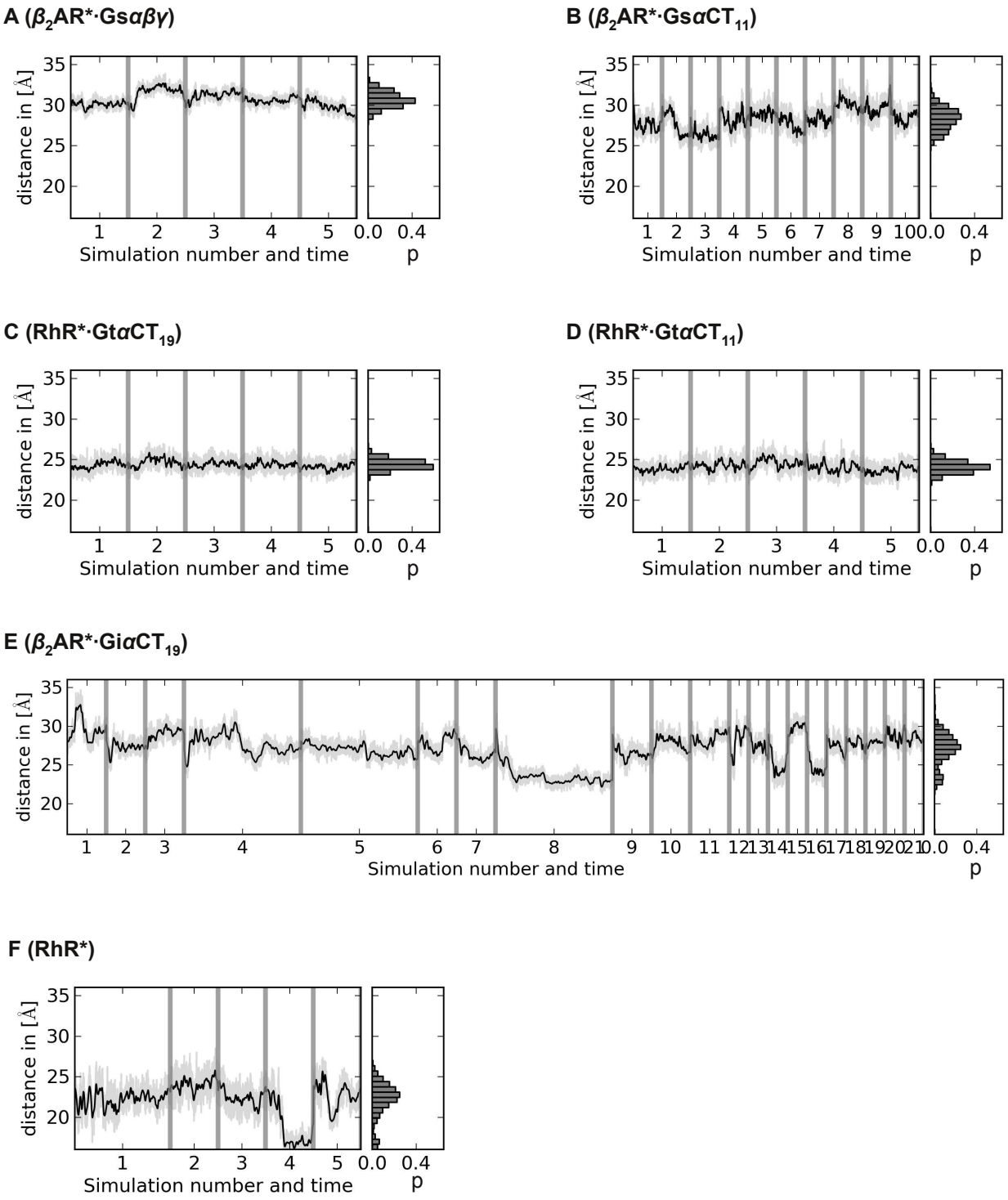

TM6 tilt measured as the TM2-TM6 distances of (**A**) β_2AR*·Gs$\alpha\beta\gamma$, (**B**) β_2AR*·GsαCT$_{19}$, (**C**) RhR*·GtαCT$_{19}$, (**D**) RhR*·GtαCT$_{11}$, (**E**) β_2AR*·GiαCT$_{19}$ and (**F**) RhR*. Shown are the time traces of the TM2-6 distances and the resulting distributions with observed probabilities p. The lengths of the individual simulations are given in Table S1. Note that N-terminal truncation to GsαCT$_{11}$ leads to higher observed variability of TM6 tilts compared to β_2AR*·GsαCT$_{19}$ or β_2AR*·Gs$\alpha\beta\gamma$, especially within individual simulations. This effect is less articulate for RhR*•GtαCT$_{11}$ compared to GtαCT$_{19}$.

Figure S3

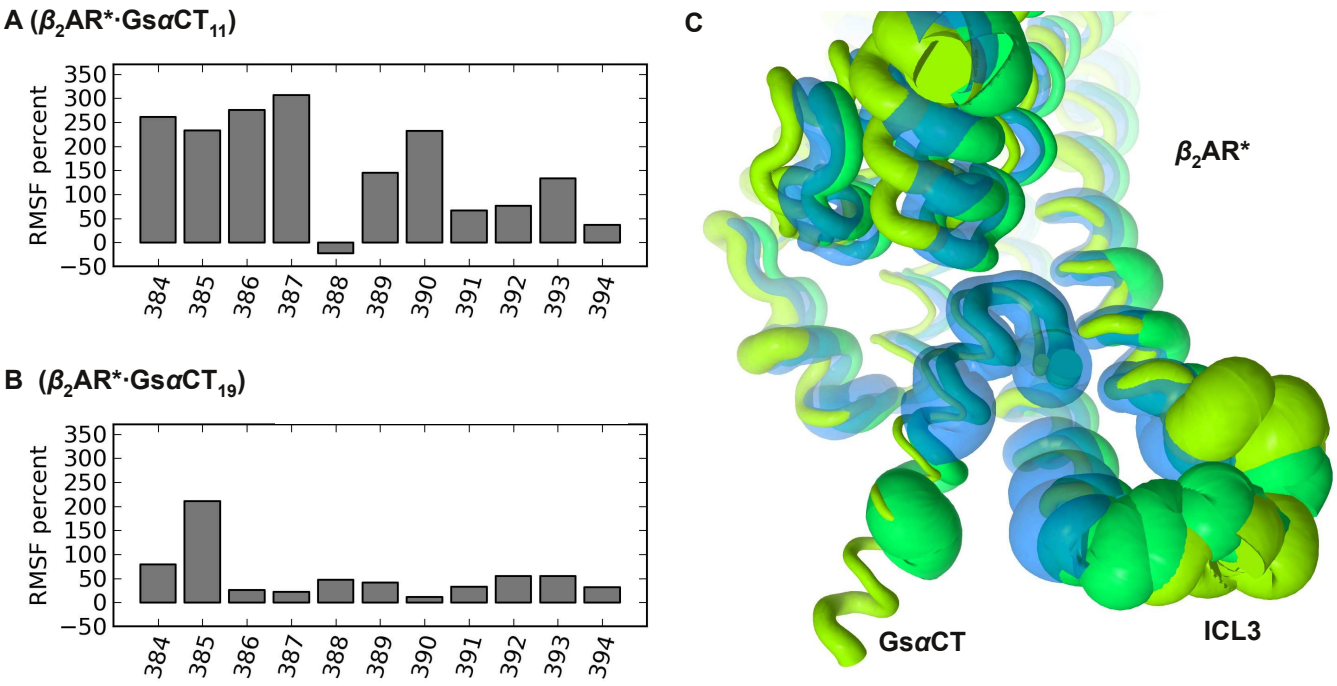

GsαCT and ICL3 flexibility of various complexes. Shown are the backbone root mean square fluctuations (RMSF) changes of GsαCT relative to β_2AR*·Gs$\alpha\beta\gamma$ of (**A**) β_2AR*·GsαCT$_{11}$ or (**B**) β_2AR*·GsαCT$_{19}$. (**C**) Tube depiction of β_2AR* with GsαCT$_{11}$ (blue), with GsαCT$_{19}$ (green) or with GsαCT from Gs$\alpha\beta\gamma$ (yellow). The thickness of the tube corresponds to the RMSF value of the respective amino acids. The RMSF is the standard deviation of atomic positions over simulation time and was calculated with the GROMACS tool g_rmsf from the MD simulations of the respective systems as listed in Table S1. Before the analysis each frame was superposed with the backbone atoms of TM 1-7 of the MD starting structure.

Figure S4

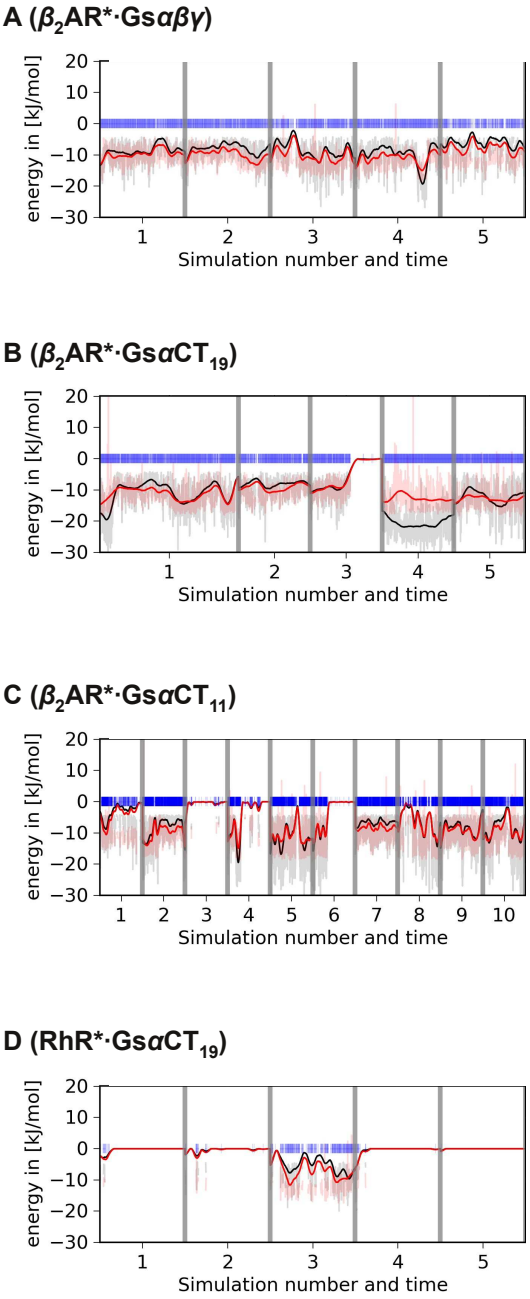

Cation-π interactions between β_2AR* and (**A**) Gs$\alpha\beta\gamma$, (**B**) GsαCT$_{19}$, (**C**) GsαCT$_{11}$ and between (**D**) RhR* and GsαCT$_{19}$. Each plot shows the data of multiple MD simulations, each between 200 and 500 ns long. See Table 1 for the lengths of the individual simulations. The timeseries show the electrostatic (black) and hydrophobic (red, Lenard-Jones potential) contributions to the interaction energy as calculated by the CaPTURE program (J. P. Gallivan, D. a Dougherty, Proc Natl Acad Sci U S A 1999, 96, 9459–64.). Blue lines denote frames where the interaction energy of cation-π interaction between $R^{3.50}$ and C391 is significant, which occurs continuosly in the β_2AR* simulations with the exceptions of simulation 3 in (**B**) and simulations 3, 4, 6 in (**C**). The cation-π interaction between RhR* and GsαCT$_{19}$ seen in simulation 3 (**D**) exhibits no face-to-face orientation as in β_2AR* but rather an edge-to-face orientation.

Figure S5

A (β_2AR*·Gs$\alpha\beta\gamma$)

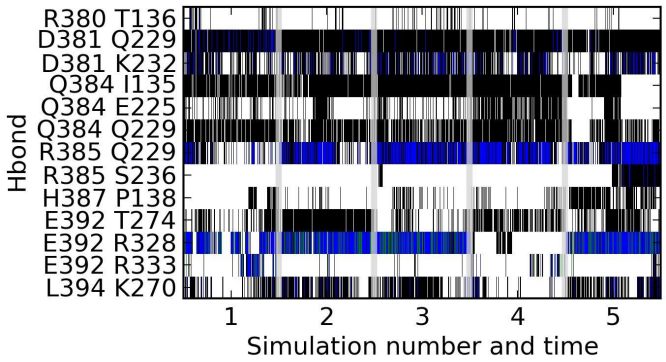

B (β_2AR*·GsαCT$_{19}$)

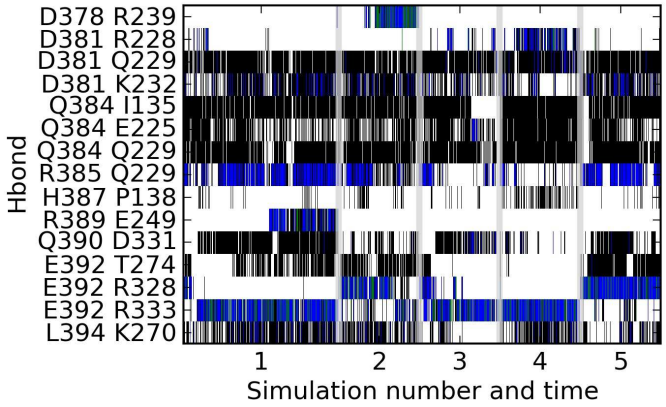

C (β_2AR*·GsαCT$_{11}$)

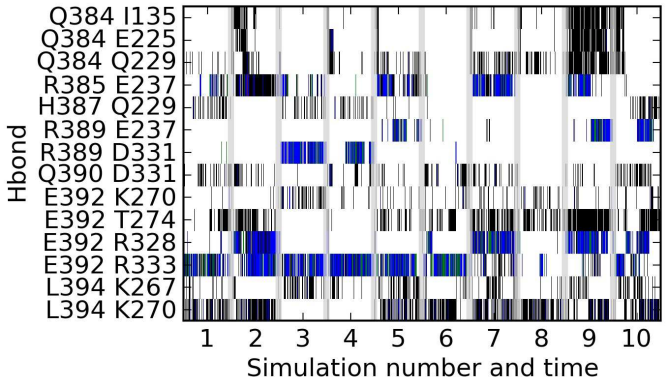

D (β_2AR*·GiαCT$_{19}$)

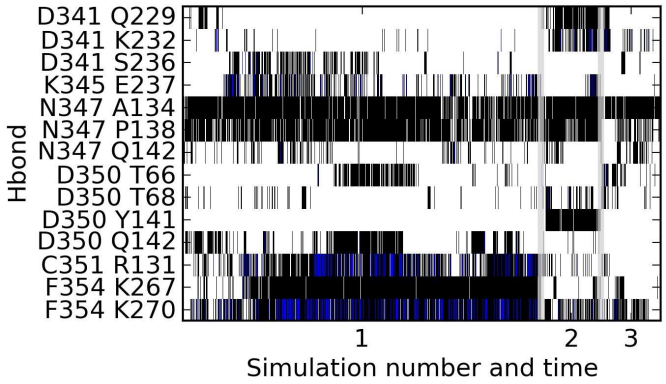

E (RhR*·GtαCT$_{19}$)

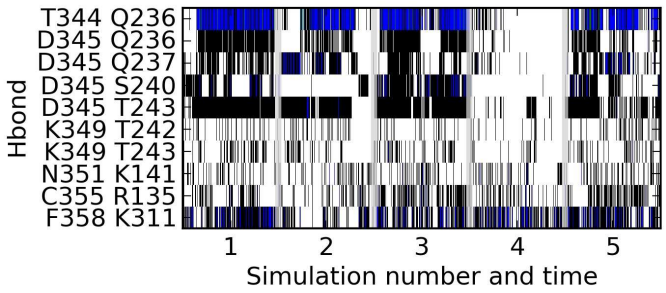

F (RhR*·GtαCT$_{11}$)

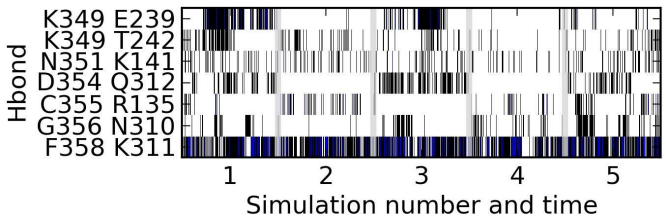

Polar interactions between R* and GαCT. Each plot shows the data of multiple MD simulation, each between 100 and 600 ns long. The lengths of the individual simulations are given in Table S1. The timeseries denote one (black), two (blue) or three (green) polar interactions between two residues as observed in the MD simulations of (**A**) β_2AR*·Gs$\alpha\beta\gamma$, (**B**) β_2AR*·GsαCT$_{19mer}$, (**C**) β_2AR*·GsαCT$_{11mer}$, (**D**) β_2AR*·GiαCT$_{19mer}$, (**E**) RhR*·GtαCT$_{19mer}$ and (**F**) RhR*·GtαCT$_{11mer}$. Polar interactions between GαCT and R* were calculated with the GROMACS tool g_hbond using a donor-acceptor distance cutoff at 3.6 Å and a cutoff angle of 30° for the angle given by the acceptor-donor-hydrogen atoms. In (**D**) only those simulations of β_2AR*·GiαCT$_{19mer}$ are shown where TM6 changes its starting position and moves inward.

Figure S6

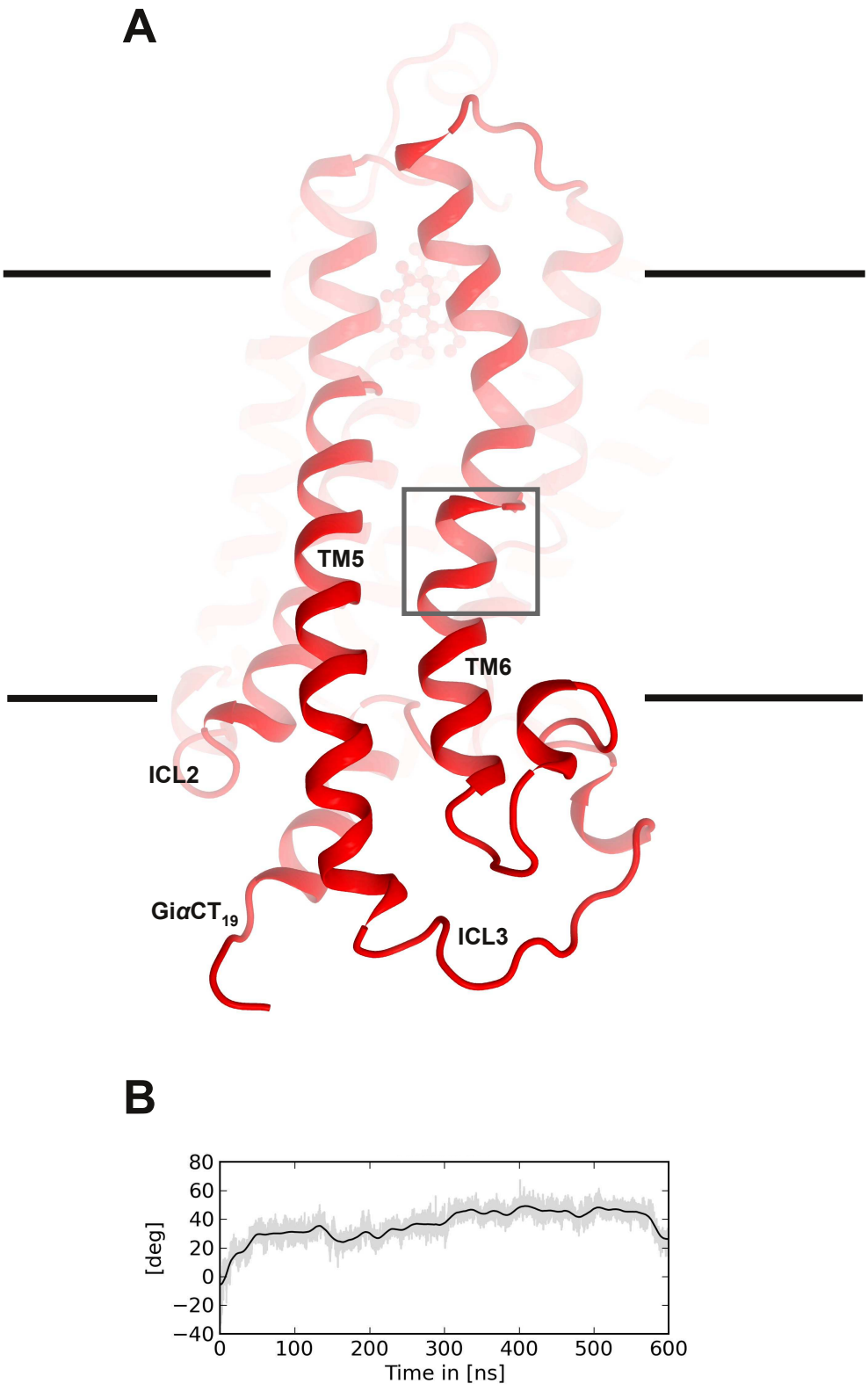

(**A**) Structuring of ICL3 that accompanies TM6 inward movement (see Fig. 2C) in the MD simulation of β_2AR*·GiαCT$_{19}$ used in the Umbrella Sampling. (**B**) Rotation of TM6 around its axis (at residues 273-280, grey box) observed in the same simulation.

Figure S7

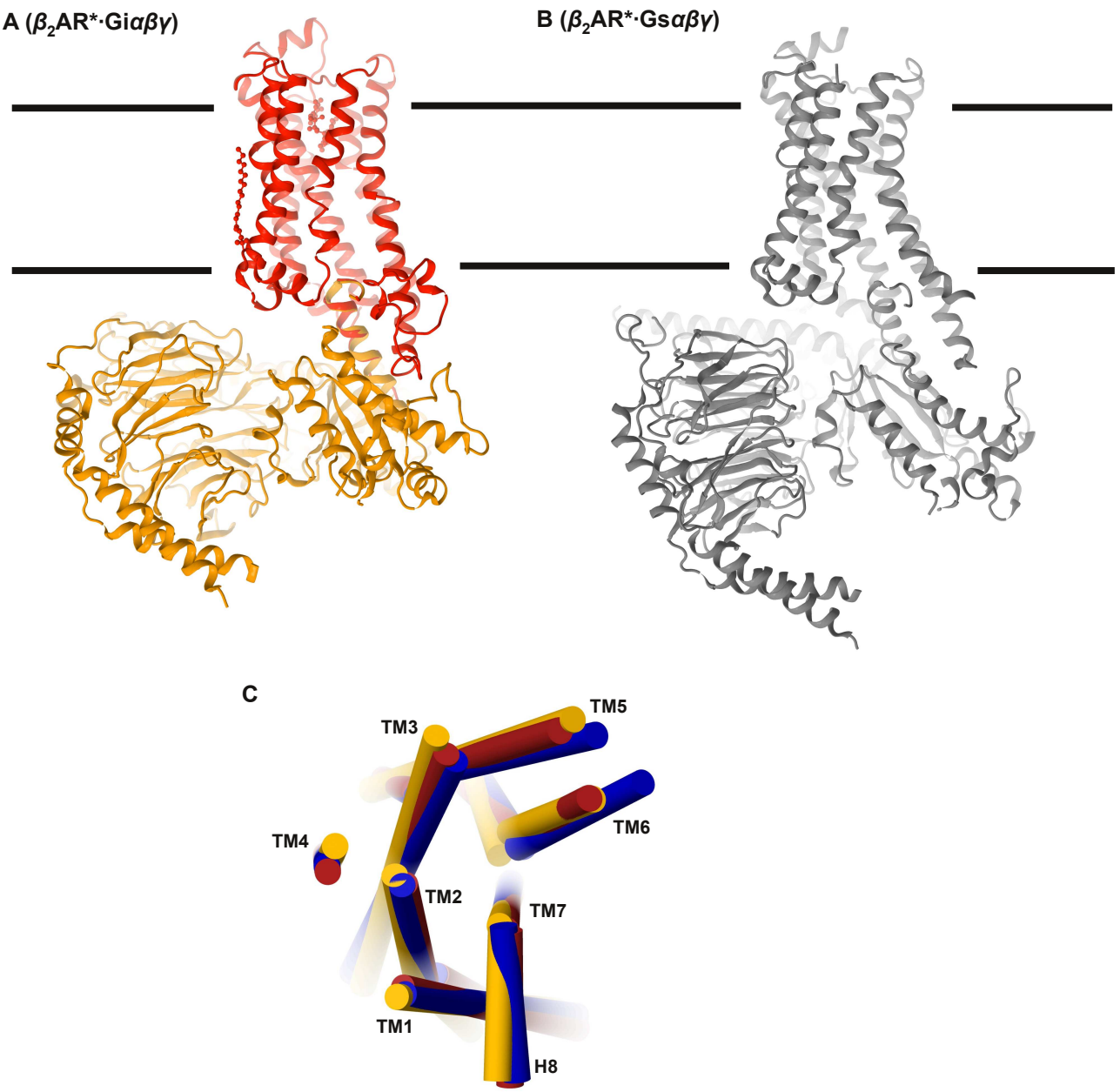

(**A**) Model of β_2AR*·Gi$\alpha\beta\gamma$ based on the arrangement of β_2AR*·GiαCT$_{19}$ determined by classical and Umbrella Sampling MD simulation data and (**B**) the crystal structure of β_2AR*·Gs$\alpha\beta\gamma$ (for comparison). Apparently there are no clashes with the membran (black lines) nor within the complex itself. As in the β_2AR·Gs holo complex, the arrangement in β_2AR·Gi does not result in any major clashes (as shown with the inactive GDP bound Gi/t in P. Scheerer et al., Nature 2008, 455, 497–502.). Comparison of both complexes, however, reveals a difference in the rotational tilt of the GαCT relative to β_2AR, resulting in a slightly different orientation of Gi$\alpha\beta\gamma$ relative to the receptor. (**C**) Comparison of the transmembrane helix arrangements in β_2AR*·GiαCT$_{19}$ (red), RhR*·GtαCT$_{11}$ (orange) and β_2AR*·Gs (blue).

Figure S8

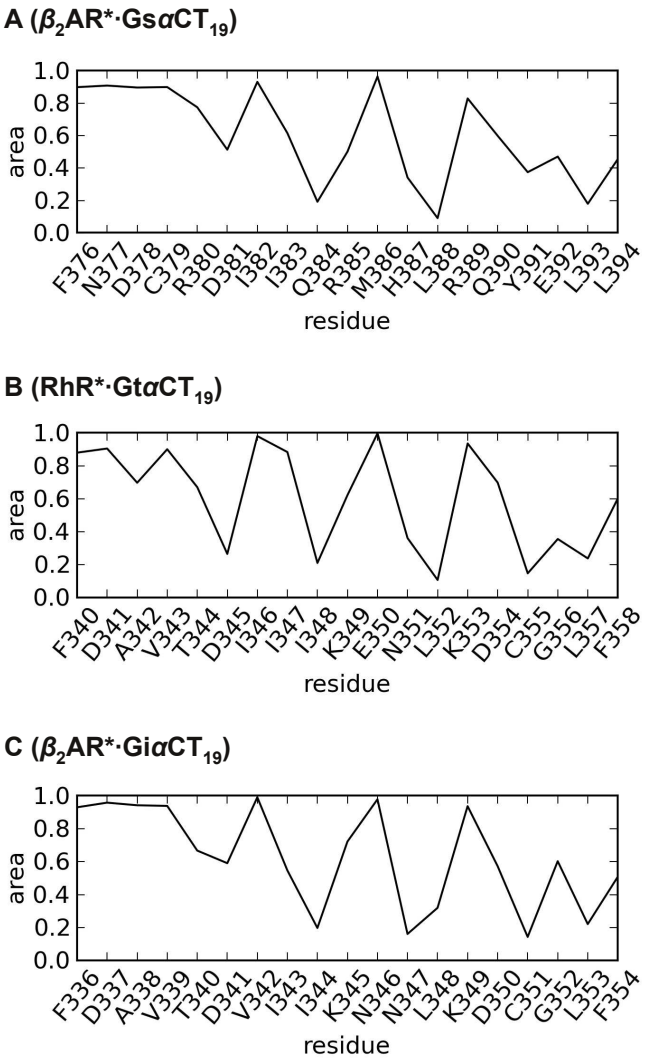

Per residue interaction area fraction of the GsαCT$_{19}$ peptides observed in MD simulations of (**A**) β_2AR*·GsαCT$_{19}$, (**B**) RhR*·GtαCT$_{19}$ and (**C**) β_2AR*·GiαCT$_{19}$. The interaction area fraction is calculated as the fraction of solvent accessible surface (SAS, calculated with the GROMACS tool g_sas) of the R*·GαCT complex and the SAS of the free peptide. A fraction of one means a residue is completely accessible whereas completely buried residues have a fraction of zero. Residues with a fraction below 0.35 are denoted buried and those with a fraction above 0.7 are denoted accessible. In (**C**) only those simulations of β_2AR*·GiαCT$_{19mer}$ are shown where TM6 changes its starting position and moves inward.

Figure S9

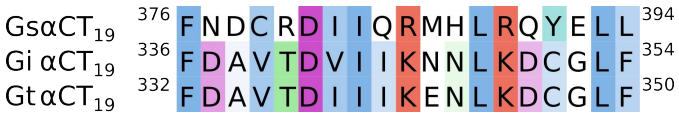

Alignment of GαCT$_{19}$ sequences colored by similarity.

Supplemental Information Methods

Preparations of active receptor (R) and GαCT structures and complexes*

The starting conformations used for MD simulations were prepared based on X-ray structures from co-crystals of β_2AR*·Gs$\alpha\beta\gamma$ (PDB entry 3SN6) [1] and of RhR*·GtαCT (PDB entry 3PQR) [2]. The far C-termini of both R* structures (RhR*: residues 327 to 348, UniProt entry P02699; β_2AR*: 342-413, UniProt entry P07550), not resolved in these complexes, were not modeled because they seem not to affect Gt activation [3].

For all simulations of β_2AR*, the coordinates from the agonist bound β_2AR*·Gs$\alpha\beta\gamma$ complex (PDB entry 3SN6), with the T4-lysozyme removed from the N-terminus, were used. A palmitoyl chain was ligated to C341 of R*. Unresolved atoms from the side chains of residues 63, 97-99, 101, 149, 175, 192-195, 267, 269-272, 299, 301-302, 304, 306 and 333 were added applying the standard geometries from the Dunbrack 2002 library [4]. Three stabilizing mutants (M96T, M98T and N187E) in β_2AR* were changed back to the wild-type form. The coordinates for the missing residues of the extracellular loop (ECL) 2 (176-178) were taken from the β_2AR* structure (PDB entry 3P0G) where ECL 2 is resolved [5]. The conformation of residues 240 to 264 from the intracellular loop (ICL) 3, which are not critical to receptor function [6], were modeled with help of the fragment based loop modeling program SuperLooper [7].

Gs$\alpha\beta\gamma$ was prepared as follows. The missing Gsα N-terminal residues 1-8 were modeled using standard geometries before a palmitoyl chain was ligated to C3 and G2 [8]. A geranylgeranyl chain was ligated to residue 68 of the Gsγ-subunit [9], after the missing residues 1-4 of the N-terminus and 63-68 of the C-terminus were added. The mutated residues G72S in Gsα and M1Q in the Gsβ were changed back to the wild-type form. Unresolved atoms from the side chains of residues 24, 35, 58, 59, 94, 118, 136, 139, 188, 189, 191, 194, 195, 201, 216, 240, 300, 322, 369 in Gsα, 1, 42, 129, 130, 172 in Gsβ and 62 in Gsγ were added using standard geometries from the Dunbrack 2002 library [4]. The conformation of the missing residues 60-70, 85-87, 203-204 and 256-262 in Gsα, were again modeled with SuperLooper [7].

For all MD simulations of RhR* two palmitoyl chains were attached to the residues C322 and C323. The coordinates from the double high-affinity K341L, C347V peptide variant in complex with RhR* (PDB entry 3PQR) were used. After back mutation of these two residues, RhR* in complex with native 11-mer Gt*α*CT was obtained (340-350). For simulations of 19-mer Gt*α*CT (332-350) the 11-mer Gt*α*CT was extended N-terminally by 8 amino acids using the geometries of an ideal *α*-helix. For simulations of 11-mer Gs*α*CT (residues 384-394) and 19-mer Gs*α*CT (residues 376-394) the coordinates from the β_2AR*·Gs*αβγ* complex were used.

Protonation states and internal water

The C-termini of Gs*α*CT, Gt*α*CT, Gi*α*CT, RhR* and β_2AR* were deprotonated (COO^-), whereas the N-termini were fully protonated ($NH3^+$). In RhR*, D83 [10,11], E113 [12], E122 [11] and E134 [13] were protonated. In β_2AR*, E122 was protonated, because it is in close contact with the hydrophobic lipid tails in the middle of the lipid bilayer (as suggested by Dror et al. [14]). All other protonation states were defined according to their respective pKa values (provided by GROMACS).

Empty polar water sized internal cavities were filled with water molecules by means of the program DOWSER [15].

Preparation of the β_2AR·Gi*αCT complex*

The β_2AR*·Gi*α*CT_{19} complex was created from MD simulations based on the crystal structure complexes of β_2AR*·Gsαβγ (PDB entry 3SN6) and RhR*·Gt*α*CT (PDB entry 3PQR). The Gi*α*CT_{19} starting position within the β_2AR* binding crevice was obtained from a superposition with the RhR*·Gt*α*CT complex. The superposition was guided by a sequence alignment of β_2AR and RhR* and employed the C*α* atoms from TM1-5 and TM7. Gi*α*CT was obtained from Gt*α*CT by changing I338 to V. With this starting position, no contacts are formed with TM6. The peptide is initially attached to ICL2 and TM5, but allowed to move freely within the R* binding crevice. In the simulations where TM6 tilts inwards (Fig. 2C, S2E) the cytoplasmic crevice closes and a tight interaction is formed with TM6 (Fig. 3B, S5D).

Preparation of the RhR·GsαCT complex*

The Gs*α*CT starting position for the RhR*·Gs*α*CT complex was obtained following the same sequence alignment and superposition protocol as for β_2AR*·Gi*α*CT but with RhR* as the receptor and Gs*α*CT as the peptide target.

Molecular dynamics protocol

System preparation and subsequent minimization and equilibration were performed with the GROMACS suite (version 4.5) [16]. The proteins were inserted into the equilibrated bilayer of dimyristoylphosphatidylcholine (DMPC) using the GROMACS g_membed tool [17]. Parameters for the DMPC lipids were derived from Berger et al. [18] and for water from the SPC/E model [19]. A salt concentration of 0.15 mol/L was obtained by adding Na^+ and Cl^- ions to the system with the GROMACS tool genion. The AMBER99SB-ILDN force field [20] was used for proteins and ions. Ligand parameters for the agonist *5-hydroxy-4H-benzo[1,4]oxazin-3-one* (a.k.a. BI-167107) of β_2AR* were created with the PRODRG2 webserver [21]. Parameters for the deprotonated *all-trans retinal* in RhR* were adapted from Mertz et al. [22]

To obtain clash-free structures suitable for MD simulations, an energy minimization was performed in GROMACS using the steepest descent algorithm until the maximum force went below 1000.0 kJ/mol/nm. In the following equilibration step the energy minimized structure was simulated for 20 ns with all protein backbone atoms restrained to their initial positions. This allows for relaxation at the protein-membrane, protein-water and the membrane-water interfaces so that voids are filled and side chain packing is optimized. For the production MD simulations the position restraints were lifted.

Based on the equilibrated systems, the production runs were started with different initial velocities obtained from Boltzmann distributions at 320 K. For equilibration and the production runs all bonds were constrained using the LINCS algorithm [23], with the exception of water bonds, which were constrained by the SETTLE algorithm [24]. The temperature was kept constant by coupling the system to a temperature bath of 320 K, which is high enough to keep the DMPC membrane from entering the gel phase. The temperature coupling was performed using the velocity-rescaling thermostat of Bussi et al. [25] with a time constant of 0.2 ps. Long range electrostatics

were calculated with the PME method [26]. Berendsen pressure coupling was performed with a time constant of 2.0 ps and semi-isotropic scaling separating scaling in the membrane plane directions from the z-direction (i.e the membrane plane normal). The integration time step used for all simulations was 0.002 ps.

Umbrella sampling

Umbrella sampling (US) facilitates sampling of the conformational space by applying a restraining potential along a transition coordinate. By employing umbrella sampling over a series of windows a range of the transition coordinates can be sampled which would be inaccessible to direct sampling due to energy barriers of the transition coordinate. The resulting series of histograms contains the biased distribution along the transition coordinate. The weighted histogram analysis method is employed to unbias and combine the histograms [27]. From the resulting distribution the potential of mean force can be calculated as $PMF(c) = -k_B T \ln \langle p(c) \rangle$ for the probability p of the transition coordinate c.

Here, the transition coordinate for the free energy calculations of TM6 inward movement and β_2AR* GiαCT interaction was selected from the trajectories of a series of β_2AR*·GiαCT$_{19\text{-mer}}$ MD simulations (Fig. S2E, simulation 8). Along the selected trajectory, umbrella sampling MD simulations were performed with respect to the TM6 inward transition, by applying the umbrella potential to the upper part of TM6, namely to the backbone atoms of residues 265 to 277. We simulated 36 US windows for 200 ns, each. WHAM was then employed to obtain the PMFs from the last 100 ns from each US window and the error was estimated by the standard deviation of a block-wise (three equally sized blocks) analysis.

TM6 tilt

The distance between TM2 and 6 ($d_{TM2\text{-}6}$) was used as an indicator of the TM6 tilt. It is measured as the distance between the geometric centers for intracellular sections of TM2 and TM6. For TM2 we used the backbone atom positions of the residues 71-75 (RhR*) and 67-71 (β_2AR*); for TM6 244-248 and 265-269, respectively.

References

[1] S. G. F. Rasmussen, B. T. Devree, Y. Zou, A. C. Kruse, K. Y. Chung, T. S. Kobilka, F. S. Thian, P. S. Chae, E. Pardon, D. Calinski, et al., *Nature* **2011**, *450*, 383–387.

[2] H.-W. Choe, Y. J. Kim, J. H. Park, T. Morizumi, E. F. Pai, N. Krauss, K. P. Hofmann, P. Scheerer, O. P. Ernst, *Nature* **2011**, *471*, 651–5.

[3] J. Chen, C. L. Makino, N. S. Peachey, D. A. Baylor, M. I. Simon, *Science* **1995**, *267*, 374–7.

[4] R. L. Dunbrack, F. E. Cohen, *Protein Sci* **1997**, *6*, 1661–81.

[5] S. G. F. Rasmussen, H.-J. Choi, J. J. Fung, E. Pardon, P. Casarosa, P. S. Chae, B. T. Devree, D. M. Rosenbaum, F. S. Thian, T. S. Kobilka, et al., *Nature* **2011**, *469*, 175–180.

[6] R. C. Rubenstein, S. K. Wong, E. M. Ross, *J Biol Chem* **1987**, *262*, 16655–16662.

[7] P. W. Hildebrand, A. Goede, R. A. Bauer, B. Gruening, J. Ismer, E. Michalsky, R. Preissner, *Nucleic Acids Res.* **2009**, *37*, W571–4.

[8] C. Kleuss, E. Krause, *EMBO J.* **2003**, *22*, 826–32.

[9] P. B. Wedegaertner, P. T. Wilson, H. R. Bourne, *J. Biol. Chem.* **1995**, *270*, 503–6.

[10] P. Rath, L. DeCaluwe, P. Bovee-Geurts, *Biochemistry* **1993**, *32*.

[11] K. Fahmy, F. Jager, M. Beck, T. A. Zvyaga, T. P. Sakmar, F. Siebert, *Proc. Natl. Acad. Sci. USA* **1993**, *90*, 10206–10210.

[12] F. Jaeger, K. Fahmy, T. Sakmar, *Biochemistry* **1994**, *33*, 10878–10882.

[13] K. Fahmy, T. Sakmar, F. Siebert, *Biochemistry* **2000**, *39*, 10607–10612.

[14] R. O. Dror, D. H. Arlow, D. W. Borhani, M. Ø. Jensen, S. Piana, D. E. Shaw, *Proc Natl Acad Sci U S A* **2009**, *106*, 4689–4694.

[15] L. Zhang, J. Hermans, *Proteins* **1996**, *24*, 433–8.

[16] B. Hess, C. Kutzner, D. van der Spoel, E. Lindahl, *J. Chem. Theory Comput.* **2008**, *4*, 435–447.

[17] M. G. Wolf, M. Hoefling, C. Aponte-Santamaría, H. Grubmüller, G. Groenhof, *J. Comput. Chem.* **2010**, *31*, 2169–74.

[18] O. Berger, O. Edholm, *Biophys. J.* **1997**, *72*, 2002–2013.

[19] H. J. C. Berendsen, J. R. Grigera, T. P. Straatsma, *J. Phys. Chem.* **1987**, *91*, 6269–6271.

[20] K. Lindorff-Larsen, S. Piana, K. Palmo, P. Maragakis, J. L. Klepeis, R. O. Dror, D. E. Shaw, *Proteins* **2010**, *78*, 1950–1958.

[21] A. W. Schüttelkopf, D. M. F. van Aalten, *Acta Crystallogr. Sect. D, Biol. Crystallogr.* **2004**, *60*, 1355–1363.

[22] B. Mertz, M. Lu, M. F. Brown, S. E. Feller, *Biophys. J.* **2011**, *101*, L17–9.

[23] B. Hess, H. Bekker, H. J. C. Berendsen, J. G. E. M. Fraaije, *J. Comput. Chem.* **1997**, *18*, 1463–1472.

[24] S. Miyamoto, P. A. Kollman, *J. Comput. Chem.* **1992**, *13*, 952–962.

[25] G. Bussi, D. Donadio, M. Parrinello, *J Chem Phys* **2007**, *126*, 14101.

[26] T. Darden, D. York, L. Pedersen, *J Chem Phys* **1993**, *98*, 10089.

[27] D. Wu, *J. Chem. Phys.* **2010**, *133*, 044115.